been achieved by careful circuit design combined with recent advances in the SiGe bipolar technology.

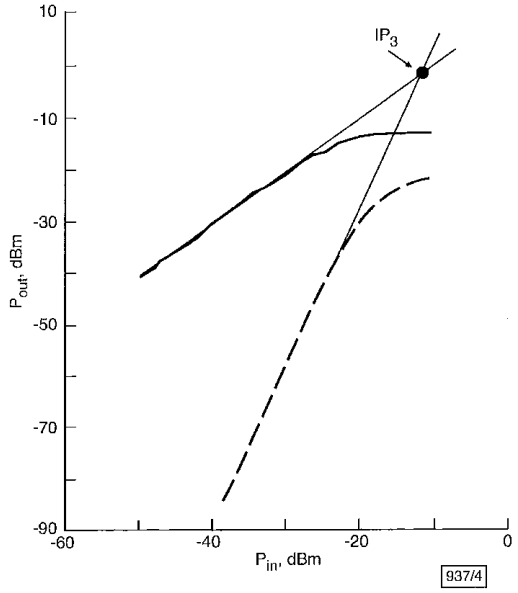


**Fig. 4** *Intermodulation performance at 20GHz*

$f_{RF1}$ = 20GHz, $f_{RF2}$ = 20.001GHz, $f_{LO}$ = 20.24GHz, $P_{LO}$ = 0dBm
——— $P_1$
– – – – $P_3$

**Table 1**: Summary of technical data

| | |
|---|---|
| 3dB bandwidth | 20GHz |
| Conversion gain (*PLO* = 0dBm) | 13dB at 2GHz<br>10dB at 20GHz |
| Double-sideband noise figure | 6dB at 20GHz |
| 1dB compression point | –21dBm at 20GHz |
| Third-order intercept point | –11.3dBm at 20GHz |
| Supply voltage range | 4.5–5.8V |
| Current (4.5V) | 2mA |
| Power consumption (4.5V) | 9mW |
| Chip size | 0.45 x 0.45mm |
| Technology | 0.5μm/80GHz $f_T$ SiGe |

*Conclusions:* A monolithically integrated active broadband mixer for wireless communications in a 0.5μm 80GHz-$f_T$ SiGe bipolar technology was presented. The mixer is optimised for a low-power and low-noise figure and operates with a conversion gain > 10 dB and up to 20GHz. To our knowledge, this is the highest operating frequency for a monolithic mixer in a silicon-based technology.


*23 October 2000*
*Electronics Letters Online No: 20010034*
*DOI: 10.1049/el:20010034*

S. Hackl, T.F. Meister, M. Wurzer, H. Knapp, K. Aufinger and L. Treitinger (*Infineon Technologies AG, Corporate Research, Otto-Hahn-Ring 6, D-81730 Munich, Germany*)

E-mail: sabine.hackl@infineon.com

A.L. Scholtz (*Institute of Communications and Radio-Frequency Engineering, Vienna University of Technology, Gußhausstraße 25/389, A-1040 Vienna*)

S. Hackl: Also with Institute of Communications and Radio-Frequency Engineering, Vienna University of Technology, Gußhausstraße 25/389, A-1040 Vienna

## References

1 DÖRR, W., ERBEN, U., SCHÜPPEN, A., DIETRICH, H., and SCHUMACHER, H.: 'Low-power low-noise active mixers for 5.7 and 11.2GHz using commercially available, SiGe HBT MMIC technology', *Electron. Lett.*, 1998, **34**, (21), pp. 1994–1996

2 GLENN, J., CASE, M., HARAME, D., MEYERSON, B., and POISSON, R.: '12-GHz Gilbert mixers using a manufacturable Si/SiGe epitaxial-base bipolar technology'. IEEE Proc. Bipolar/BiCMOS Circuits Technol. Mtg., 1995, pp. 186–189

3 OSAFUNE, K., and YAMAUCHI, Y.: '20GHz 5dB gain analog multipliers with Al-GaAs/GaAs HBTs'. IEEE MTT Symp. Dig., 1991, pp. 1282–1285

4 KOBAYASHI, K.W., GUTIERREZ-AITKEN, A., COWLES, J., TANG, B., DESROSIERS, R., MEDVEDEV, V., TRAN, L.T., BLOCK, T.R., OKI, A.K., and STREIT, D.C.: '15dB gain, DC-20GHz InP HBT balanced analog mixer and variable gain amplifier with 27dB of dynamic range'. IEEE Radio Frequency Integrated Circuits Symp., 1999, pp. 105–108

5 GILBERT, B.: 'The micromixer: a highly linear variant of the Gilbert mixer using a bisymmetric class-AB input stage', *IEEE J. Solid-State Circuits*, 1997, pp. 1412–1423

6 MEISTER, T.F., SCHÄFER, H., FRANOSCH, M., MOLZER, W., AUFINGER, K., SCHELER, U., WALZ, C., STOLZ, M., BOGUTH, S., and BÖCK, J.: 'SiGe base bipolar technology with 74GHz $f_{max}$ and 11ps gate delay'. IEEE IEDM Tech. Dig., 1995, pp. 739–742

# Microphotonic millimetre-wave receiver architecture

D.A. Cohen and A.F.J. Levi

A new microphotonic millimetre-wave receiver architecture with direct electrical-to-optical conversion is presented. The receiver uses high-Q RF and microphotonic electro-optic resonators which are operated in simultaneous resonance. Numerical simulations indicate that efficient modulation of an optical carrier at RF in the millimetre-wave range can be realised.

Radio frequency (RF) receivers operating at millimetre-wave frequencies are of interest for indoor wireless and microcell wireless systems [1]. In this Letter, we propose a novel architecture for these wireless and front-end antenna applications. By exploiting the unique properties of a microphotonic modulator, efficient, low-power detection in a small volume can be achieved.

A microphotonic optical resonator is fabricated from an electro-optic material. The optical quality-factor (Q) of the resonator is high to increase the effective interaction length of photons with an applied RF electric field. When combined with a simultaneously resonant RF electrical feed for voltage gain and a patterned electrode structure, high-sensitivity at millimetre-wave frequencies is achievable.

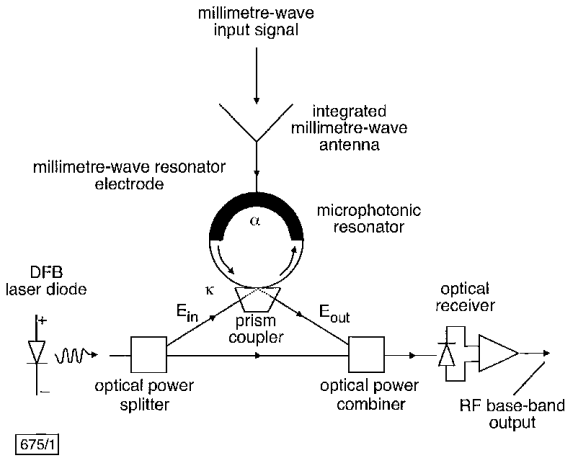


**Fig. 1** *Schematic diagram showing the receiver proposed for millimetre-wave RF detection*

Fig. 1 is a schematic diagram showing the proposed receiver. An electromagnetic wave is received at a RF antenna integrated with the modulator. This millimetre-wave signal feeds the electrodes of the microphotonic resonator where the RF signal is directly converted via the electro-optic response of the modulator to a 200THz optical carrier frequency supplied by a distributed

feedback (DFB) laser. The resulting phase-modulated optical signal is converted to amplitude-modulation through the use of a standard Mach-Zehnder configuration. The intensity of the amplitude-modulated optical carrier is detected by the optical receiver which is sensitive only to baseband frequencies.

There are many practical configurations for the microphotonic modulator. One particular approach uses a z-cut $LiNbO_3$ disk-shaped resonator with optically polished curved sidewalls and optical refractive index $n_{opt}$ = 2.14. Simultaneous resonance is achieved by confining a TE-polarised optical-field in a high-Q whispering-gallery mode along the periphery of the disk, while metal electrodes patterned above and below the disk ensure good overlap of the resonant RF and optical fields. Optical input and output may be achieved by means of standard evanescent prism-coupling with a power-coupling coefficient $\kappa$ [2].

This optical resonator design can have Qs in excess of $4 \times 10^6$, resulting in an effective photon interaction length with the RF field of > 50cm for light of wavelength 1.5μm. Although one sacrifices bandwidth with this resonant configuration, the effective photon interaction length is more than 25 times that of a conventional Mach-Zehnder $LiNbO_3$ modulator.

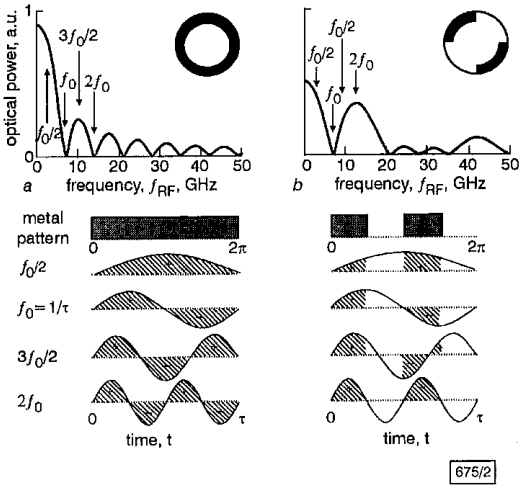


**Fig. 2** *Calculated response of microphotonic-based opto-electronic modulator with the indicated periodic metal-electrode structures, $f_0$ = 7GHz and τ = 142ps*

*a* $R$ = 3.18mm $LiNbO_3$ disk modulator with $\kappa$ = 1 and continuous ring-electrode
*b* $\kappa$ = 1 optical-coupling with a split four-segment ring-electrode showing a peak in opto-electronic response at 14GHz

Frequency of operation is determined by the free spectral range (FSR) of the optical resonator and the spatial pattern of the metal-electrode structure. The frequency of the RF carrier $f_{RF}$ should be an integral multiple $m$ of the optical FSR such that $f_0 = 1/\tau_{disk} = n_{opt}2\pi R/c$ where $\tau_{disk}$ is the optical round-trip time of the disk and $R$ is the disk radius. A periodic metal-electrode structure permits operation of the modulator well beyond a typically 20GHz –3dB roll-off of conventional commercial $LiNbO_3$ modulators. This is understood by first considering an ideal single optical-pass configuration ($\kappa$ = 1). The modulation response of a solid-ring electrode is just that of a conventional Mach-Zehnder interferometer (Fig. 2*a*). We assume a radius $R$ = 3.18mm which gives a FSR of $f_0$ = 7.03GHz. As expected, the modulator has a sinc-function response with little efficiency at large values of $f_{RF}$. The first null in the frequency response is when the round-trip time of the optical wave $\tau_{disk}$ equals the period $T = 1/f_{RF}$. This occurs because during the positive part of the electric-field cycle of the RF, the optical field of the disk obtains a positive phase-shift ('+' in Fig. 2) which is exactly cancelled during the negative cycle ('–' in Fig. 2). Similarly, when the applied RF frequency is any integer multiple $m$ of the optical round-trip frequency ($f_{RF} = m/\tau_{disk}$), a null in the frequency response results. Modulation can be enhanced at such a null if the electrode structure is modified as, for example, shown in Fig. 2*b*. In this case, while the RF electric-field at frequency $f_{RF} = 2f_0$ is positive, light passing through a region with an electrode receives a positive phase-shift. While the RF electric field is negative, the light passes through a region without an electrode and receives no phase-shift. Results of calculations given in Fig. 2*b* show that the use of the patterned electrode enables efficient modulation near 14GHz. The loss in baseband efficiency, compared to the baseband response of the solid-ring electrode shown in Fig. 2*a*, is a result of only half the disk being patterned.

In its simplest form, the periodic electrode concept is designed for frequencies $f_{RF} = mf_0$, with a corresponding number of $m$ equally spaced metal sections, each covering a fraction $1/2m$ of the circumference of the disk.

For the optically resonant case ($\kappa$ < 1), the modulated optical electric field resulting from multiple round-trips is given by the expression

$$E_{out}(t) = \left[\sqrt{(1-\kappa)}E_{in}(t) - \frac{\kappa}{\sqrt{(1-\kappa)}}\sum_{j=1}^{\infty} r^j e^{-iF_n(t-j\tau_{disk})}E_{in}(t-j\tau_{disk})\right]$$

$$F_j(t-j\tau_{disk}) = \left[\sum_{k=0}^{j-1}\phi(t-k\tau_{disk})\right]$$

where $E_{out}(t)$ is the electric field exiting the prism, $E_{in}(t)$ is the field entering the prism, $n$ is the round-trip number, $r = \alpha^{1/2}(1-\kappa)^{1/2}$, $\alpha$ is the optical singlepass power transmission, and $\phi(t)$ is the optical singlepass phase-shift resulting from the applied RF field.

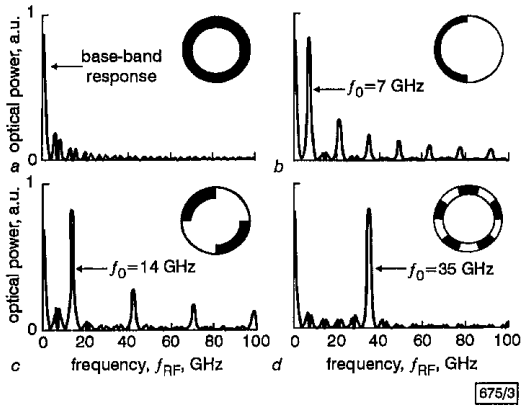


**Fig. 3** *Calculated response of microphotonic-based opto-electronic modulator with indicated periodic metal electrode structures*

*a* $R$ = 3.18mm $LiNbO_3$ disk modulator with $\kappa$ = 0.5 and continuous ring electrode
*b* $\kappa$ = 0.5 with a split two-segment ring-electrode showing resonant opto-electronic response at 7GHz
*c* $\kappa$ = 0.5 with four segments and response at 14GHz
*d* $\kappa$ = 0.5 with 10 segments showing response at 35GHz

For the resonant solid-ring electrode, the high-Q results in a summation of multiple round-trips that further suppresses modulation efficiency. Figs. 3*b* and *d* show how a change in metal-electrode pattern shifts the resonant response to higher frequencies with little decrease in efficiency. This demonstrates that disk size, in itself, does not limit millimetre-wave operation.

The relative response at the resonant frequency compared to baseband is unity indicating the potential for efficient modulation. When integrated with a RF voltage resonator circuit attached to the antenna, the effective power gain of the receiver can be large.

In conclusion, a new type of millimetre-wave RF receiver architecture with direct electrical-to-optical conversion has been described. Numerical simulation of a microphotonic modulator which uses simultaneous resonance of optical and RF electric-fields has demonstrated that efficient modulation is achievable at millimetre-wave frequencies through the use of a periodic metal electrode.

*Acknowledgment:* This work is supported in part by the National Science Foundation under contract ECS-9979331 and the DARPA RFLICs program.

5 October 2000
*Electronics Letters Online No: 20010038*
*DOI: 10.1049/el:20010038*

D.A. Cohen and A.F.J. Levi (*Department of Electrical Engineering, University of Southern California, Los Angeles, California, 90089-1111, USA*)

E-mail: alevi@usc.edu

### References

1 OHATA, K., INOUE, T., FUNABASHI, M., INOUE, A., TAKIMOTO, Y., KUWABARA, T., SHINOZAKI, S., MARUHASHI, K., HOSAYA, K., and NAGAI, H.: 'Sixty-GHz-band ultra-miniature monolothic T/R modules for multimedia wireless communication systems', *IEEE Trans. Microw. Theory Tech.*, 1996, **44**, pp. 2354–2360

2 TIEN, P.K., and ULRICH, R.: 'Theory of prism-film coupler and thin-film light guides', *J. Opt. Soc. Am.*, 1970, **60**, pp. 1325–1337

## Source-controlled channel decoding using nonbinary turbo codes

Zhaohui Cai, K.R. Subramanian and Liren Zhang

The residual redundancy contained in the source coding output symbols can be used by the channel decoder to provide extra error protection. A joint source/channel coding scheme which employs nonbinary turbo codes over rings to exploit the residual redundancy of source coding output is investigated. Simulation results on codebook-excited linear predictive coded speech and differential pulse code modulation coded image transmissions over noisy channels are presented.

*Introduction:* It has been shown that the residual redundancy contained in the output symbols of source coding can be used by (channel) turbo codes to provide further error protection in additive white Gaussian noise (AWGN) channels [1]. In [2] Sayood *et al.* suggest that the residual redundancy can be utilised more efficiently when source and channel encoder share an alphabet. In this Letter, we apply nonbinary turbo codes over ring $Z_M$ to utilise the residual redundancy of source-coding outputs. Turbo codes are well known because they can achieve almost reliable communication at signal-to-noise ratios (SNR) very close to the Shannon-limit and there exists an iterative symbol-by-symbol maximum *a posteriori* probability (MAP) decoding scheme with moderate complexity [3]. The component codes of turbo codes, i.e. binary recursive systematic convolutional (RSC) codes, can be generalised to nonbinary codes over rings [4]. In this work we extend the source-controlled channel decoding to the nonbinary case and propose a modification of conventional MAP decoding schemes.

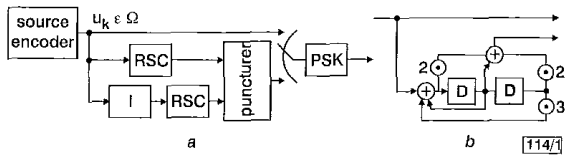


**Fig. 1** *Source/channel encoder and nonbinary RSC example*
*a* Encoder
*b* Example

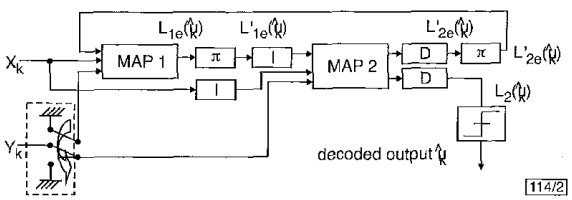


**Fig. 2** *MAP iterative decoding with knowledge of source statistics*

*System structure:* The joint source/channel encoder is shown in Fig. 1. The source encoder delivers symbols from an alphabet $\Omega = \{0, 1, ..., M-1\}$, where $M$ usually is a power of 2, i.e. $M = 2^m$. The source encoder is followed by a channel (turbo) encoder which consists of two parallel concatenated RSC component ring codes linked by a pseudorandom symbol interleaver. The source and channel encoders share the same alphabet. It has been shown in [4] that every rate $r = k/n$ convolutional code over ring $R = Z_M$ can be generated by some encoding matrix $G(D) \in R(D)^{k \times n}$, where $R(D)$ is the ring of rational functions over $R$. An example code over $Z_4$ is also shown in Fig. 1, which will be used in our simulation. The output of two RSC encoders are punctured alternatively to maintain the rate $r = 1/2$.

The simplest way to model the redundancy of source-coded symbols is the first-order Markov chain with symbol transition probability $P(u_k|u_{k-1})$. Usually we can get the transition probability statistics using some training sequence [2, 8]. The iterative MAP decoding algorithm was extended to nonbinary trellis codes in the appendix of [5]. To utilise the residual redundancy of source-coded symbols in the channel decoder, the conventional MAP decoding scheme must be modified. A simple modification is shown in Fig. 2. The structure of the decoder is similar to the conventional decoder proposed in [3], except for function modules $\pi$ introduced between two MAP decoder modules. $X_k$ and $Y_k$ are AWGN corrupted information and parity check sequence, respectively. For every information symbol $u_k$, each MAP decoder $i$ may deliver a soft output $L_i(\hat{u}_k) := \ln(P_i(u_k|\text{observation}))$ as well as an *extrinsic* output $L_{ie}(\hat{u}_k) := \ln(P_{ie}(u_k))$ which is used as *a priori* value in the subsequent iteration step [3]. For more information on notation here, and on how to decode binary/nonbinary turbo codes, refer to [3, 5]. In our scheme, $L_{ie}(\hat{u}_k)$ is updated to $L'_{ie}(\hat{u}_k)$ by module $\pi$ in Fig. 2 before it is sent to the next MAP decoder as *a priori* estimation:

$$L'_{ie}(\hat{u}_k) = \ln\left[\frac{1}{2}\left(P_{ie}(\hat{u}_k) + \sum_{\hat{u}_{k-1}} P(u_k|u_{k-1})P_{ie}(\hat{u}_{k-1})\right)\right] \quad k = 1, ..., N-1 \quad i = 1, 2$$

i.e. $P'_{ie}(\hat{u}_k)$ is the source transition probability averaged version of $P_{ie}(\hat{u}_k)$. $N$ is the size of the 'average' interleaver. The input to the next MAP decoder is determined not only by $L_{ie}(\hat{u}_k)$, the output of the current MAP decoder, but also by $P(u_k|u_{k-1})$, the first-order source characteristics. Simulation results show that quicker convergency of MAP decoding and higher fidelity of sources can be obtained through our proposed scheme.

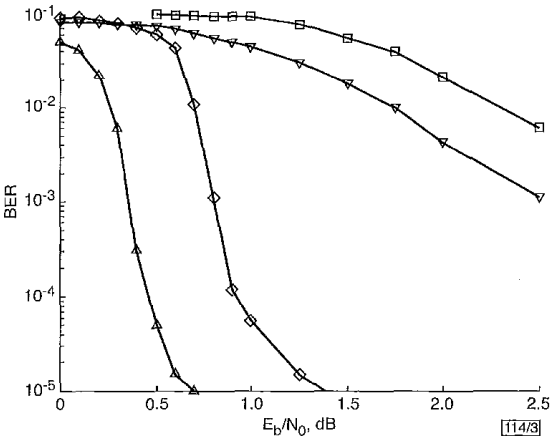


**Fig. 3** *BER performance of DPCM-coded image transmission over AWGN channel*

□— first iteration without source statistics
—◇— eighth iteration without source statistics
▽— first iteration using proposed scheme
—△— sixth iteration using proposed scheme

*Applications:* First, we apply the proposed scheme to differential pulse code modulation (DPCM)-coded image transmission. The training and testing images are 512 × 512 GIRL and COUPLE, respectively. Lloyd-Max nonuniform quantiser with $M = 2^2$ levels is used in our simulation. The nonbinary RSC code is that with $G(D) = [1, (2 + D + 2D^2)/(1 + D + 3D^2)]$, which is shown in Fig. 1. The size of the interleaver is $N = 4096 \times 2 = 8192$ bits.